Subscriber access provided by UNIV OF CALIFORNIA SAN DIEGO LIBRARIES

Article

Synchronous bioimaging of intracellular pH and chloride based on LSS fluorescent protein

Jose M. Paredes, Aurora I. Idilli, Letizia Mariotti, Gabriele Losi, Lyaysan R Arslanbaeva, Sebastian Sulis Sato, Pietro Artoni, Joanna Szczurkowska, Laura Cancedda, Gian Michele Ratto, Giorgio Carmignoto, and Daniele Arosio

ACS Chem. Biol., **Just Accepted Manuscript** • DOI: 10.1021/acschembio.6b00103 • Publication Date (Web): 31 Mar 2016

Downloaded from http://pubs.acs.org on April 1, 2016

Just Accepted

"Just Accepted" manuscripts have been peer-reviewed and accepted for publication. They are posted online prior to technical editing, formatting for publication and author proofing. The American Chemical Society provides "Just Accepted" as a free service to the research community to expedite the dissemination of scientific material as soon as possible after acceptance. "Just Accepted" manuscripts appear in full in PDF format accompanied by an HTML abstract. "Just Accepted" manuscripts have been fully peer reviewed, but should not be considered the official version of record. They are accessible to all readers and citable by the Digital Object Identifier (DOI®). "Just Accepted" is an optional service offered to authors. Therefore, the "Just Accepted" Web site may not include all articles that will be published in the journal. After a manuscript is technically edited and formatted, it will be removed from the "Just Accepted" Web site and published as an ASAP article. Note that technical editing may introduce minor changes to the manuscript text and/or graphics which could affect content, and all legal disclaimers and ethical guidelines that apply to the journal pertain. ACS cannot be held responsible for errors or consequences arising from the use of information contained in these "Just Accepted" manuscripts.

ACS Publications

ACS Chemical Biology is published by the American Chemical Society. 1155 Sixteenth Street N.W., Washington, DC 20036

Published by American Chemical Society. Copyright © American Chemical Society. However, no copyright claim is made to original U.S. Government works, or works produced by employees of any Commonwealth realm Crown government in the course of their duties.

Synchronous bioimaging of intracellular pH and chloride based on LSS fluorescent protein

Jose M. Paredes[1,3]; Aurora I. Idilli[1]; Letizia Mariotti[2]; Gabriele Losi[2]; Lyaysan R. Arslanbaeva [1,7]; Sebastian Sulis Sato[4]; Pietro Artoni[5]; Joanna Szczurkowska[6]; Laura Cancedda[6]; Gian Michele Ratto[4,5]; Giorgio Carmignoto[2]; Daniele Arosio[1,7]

[1] Institute of Biophysics, CNR, Via alla Cascata 56/C, 38123 Trento, Italy; [2] Neuroscience Institute, CNR, Viale G. Colombo 3, 35121 Padova, Italy; [3] Bruno Kessler Foundation, Via Sommarive 18, 38123 Trento, Italy; [4] Nanoscience Institute, CNR, Pisa, Italy; [5] Scuola Normale Superiore, Pisa, Italy; [6] Istituto Italiano di Tecnologia, Genoa, Italy; [7] CIBIO, University of Trento, Via delle Regole 101, 38123 Trento, Italy.

Author keywords

pH and Cl^- genetically encoded sensors; chloride; imaging; neurons; fluorescence microscopy;

ABSTRACT

Ion homeostasis regulates critical physiological processes in the living cell. Intracellular chloride concentration not only contributes in setting the membrane potential of quiescent cells, but it also plays a role in modulating the dynamic voltage changes during network activity. Dynamic chloride imaging demands new tools allowing faster acquisition rates and correct accounting of concomitant pH changes. Joining a long Stokes shift red fluorescent protein to a GFP variant with high sensitivity to pH and chloride, we obtained LSSmClopHensor, a genetically encoded fluorescent biosensor optimized for the simultaneous chloride and pH imaging and requiring only 2 excitation wavelengths (458 and 488 nm). LSSmClopHensor allowed us to monitor the dynamic changes of intracellular pH and chloride concentration during seizure like discharges in neocortical brain slices. Only cells with tightly controlled resting potential revealed a narrow distribution of chloride concentration peaking at about 5 and 8 mM, in neocortical neurons and SK-N-SH cells, respectively. We thus showed that LSSmClopHensor represents a new versatile tool for studying the dynamics of chloride and proton concentration in living systems.

Introduction

Electrochemical proton (H^+) gradients represent a ubiquitous source of energy in live cells. Chloride ion (Cl^-), the most abundant anion in organism, controls pH within cell compartments by shunting the effects of H^+ charge accumulation on membrane potential[1–3]. The importance of Cl^- in cell functions was not fully recognized until recently, yet Cl^- and H^+ play coordinated roles in physiological processes including control of membrane potential[4], regulation of cell volume[5,6], growth and migration of neurons[7–9] and synaptic signaling in both the depolarizing and hyperpolarizing directions[10,11]. Intracellular Cl^- concentration is tightly regulated by the interaction of energy-dependent transporters with passive-diffusion channels so that a gradient of varying intensity over time is established across the plasma membrane[12]. Cl^- homeostasis is of high significance in the physiopathology of many human diseases such as cystic fibrosis, myotonia, epilepsy, lysosomal storage diseases[13] and neurodevelopmental disorders[14] including autism[15], fragile X syndrome[16] and down syndrome[17]. Therefore, understanding the regulatory mechanisms of Cl^- homeostasis is of fundamental importance.

Development of experimental noninvasive means - mainly optogenetics - to monitor and manipulate intracellular Cl^- in live cells is a flourishing field with a growing number of different approaches reported in the recent literature[18–20]. The measurement of Cl^- in living cells has experienced an extraordinary development following the adoption of methods based on imaging techniques. Organic fluorescent dyes and later genetically encoded fluorescent proteins (FP) replaced the use of ion-selective electrodes[21,22]. It was the discovery of Cl^- sensitivity of yellow fluorescent protein (YFP)[23] which triggered this intense development. Combining two fluorescence proteins with distinct colors into a single construct, ratiometric biosensors were developed with the advantage of being free from the influence of local probe

concentration, thickness of the specimen, light scattering, illumination intensity fluctuation, and photobleaching[24]. Chloride biosensors can be based on the fluorescence resonance energy transfer (FRET) between a CFP variant and a chloride-binding YFP variant; in this case, they are ratiometric in emission[24–26]. Unfortunately, FRET-based Cl^- measurements are biased by a strong pH dependency - present in all the YFP and GFP variants adopted in chloride-sensing applications - of both the Cl^- binding affinity and the emitted fluorescence[27]. Precise Cl^- measurements require therefore independent estimation of the intracellular pH[28,29] or, alternatively, the simultaneous measurement of intracellular Cl^- and pH combined into a single construct[30]. Based on the pH and Cl^- independent fluorescence of DsRed-monomer, ClopHensor prevents the intricate pH dependency of FRET signals and provides both a chloride-independent ratiometric measurement of the intracellular pH and an accurate measurement of the intracellular Cl^- concentration. ClopHensor is ratiometric in excitation and requires, for its operation, sequential illumination with three wavelengths to excite the pH isosbestic point at exactly 458 nm, the green anionic form at about 488 – 500 nm and the red component at about 540 – 560 nm. The requirement of three excitation wavelengths limited the use of ClopHensor to dedicated setups despite the increasing interest in accurate mapping of Cl^- fluxes in the dendritic tree and cell body of neurons in intact brain under both physiological conditions[31,32] and in animal models of neuronal disorders[33,34].

To simplify setup requirements and allow a wider adoption of quantitative chloride imaging with the correct analysis of concomitant pH changes, we reasoned whether it was possible to substitute DsRed-monomer with a FP with a large (> 100 nm) Stokes shift. Red fluorescence proteins with a large distance between excitation and emission maxima could allow the ratiometric operation using a single excitation wavelength that is optimal for both the green and red proteins. Here, we tested LSSmKate2[35,36] as a partner of E^2GFP, a GFP variant that

contains a highly specific Cl^- binding site[37]. We named the new biosensor LSSmClopHensor, and demonstrated its ability to perform dynamic measurement of concomitant changes of intracellular H^+ and Cl^- concentration in neurons.

RESULTS AND DISCUSSION

Development of LSSmClopHensor. LSSmKate2 shows favorable properties to replace DsRed-monomer in ClopHensor. LSSmKate2 excitation maximum at 460 nm matches E^2GFP isosbestic point at 458 nm[30,38] (Supplementary Figure S1); compared to DsRed-monomer, LSSmKate2 shows faster maturation rate and higher pH stability (pK_a = 2.7) with unaltered brightness.

To examine whether the fluorescence of LSSmKate2 was also stable over changes of Cl^- concentration, we purified recombinant LSSmKate2 from bacterial lysate and measured fluorescence properties. Emission spectra collected in a wide range of Cl^- concentration (from 0 to 1 M) and pH values (from 5.2 to 8.4) resulted superimposed (Supplementary Figure S2 and S3) indicating high Cl^- stability over a wide pH range. Using recombinant LSSmKate2, we also surveyed its brightness - as the product of absorption and quantum yield - relative to E^2GFP and obtained a value of 0.57 ± 0.05 (Supplementary Figure S4 and S5); a substantial improvement over the corresponding value of 0.13 for DsRed-monomer[39], which should lead to numerically more stable ratio calculation. Motivated by the large Stokes shift and the high pH and Cl^- stability of LSSmKate2, we then decided to replace DsRed-monomer with LSSmKate2 and generate LSSmClopHensor, a new chimeric protein linking E^2GFP with LSSmKate2 (Figure 1a). We expressed and purified recombinant LSSmClopHensor to check whether the chimeric protein conserved the fluorescence properties E^2GFP. The excitation wavelength (isosbestic point) that produces a pH-independent fluorescence intensity was present in the same position of E^2GFP (Figure 1b). Therefore, excitation of LSSmClopHensor at 458 nm shall continue to provide the pH-independent fluorescence signal, which turned out convenient for the simultaneous ratiometric measurement of pH and Cl^- concentration[30]. We

performed a pH titration of recombinant LSSmClopHensor in the range from 5.6 to 8.7. The ratio (488-over-458) of the emission spectra integrated from 500 to 550 nm and collected using excitation bands peaking at 488 nm (Figure 1c) and 458 nm (Figure 1d) defined the R_{pH} ratio (Figure 1e). Notably, the R_{pH} ratio is not affected by changes in Cl^- concentration, follows a single site binding curve (Methods, eq. 2) and thus allows for accurate pH measurements independently of Cl^- and LSSmClopHensor concentrations.

We then calculated the emission ratio R_{Cl} between the green (from 500 to 550 nm) and red (from 580 to 640 nm) fluorescence at increasing Cl^- concentrations using a single excitation band (Figure 1f). Increasing amount of Cl^- quenched the green fluorescence because of the static quenching mechanism that regulates Cl^- binding to the E^2GFP moiety. Red fluorescence instead remained constant thanks to the chloride-independent fluorescence of LSSmKate2. Overall, chloride titrations at various pH values demonstrated a high sensitivity for Cl^- within the physiological pH range (Figure 1g and Supplementary Figure S6). Finally, we investigated the ion shield effects on our measurements. In the cellular environment, in fact, biological processes produce continuous changes of the local ion concentrations, which can prevent correct pH measurements by altering the apparent pK_a of the sensor[40,41]. We measured the apparent pK_a of LSSmClopHensor at increasing ionic strength and observed only a slight decrease, from 6.74 ± 0.02 to 6.57 ± 0.04, when moving from low (1 mM) to high (2 M) salt concentration (Supplementary Figure S7). This assured us that LSSmClopHensor can report intracellular pH accurately even in the presence of the largest physiological changes of ion concentration.

Chloride imaging in live cells. We first expressed LSSmClopHensor in human embryonic kidney 293 (HEK293) and in human neuroblastoma (SK-N-SH)[42,43] cells. Protein expression showed a uniform distribution pattern within all cell compartments without observable

aggregates for both cell lines as well as for differentiated SK-N-SH cells - adopting neuronal-like phenotype - (Supplementary Figures S8-S10). By ionophore clamping cells at values encompassing a wide range of pH and Cl^- concentrations, we performed an *in situ* calibration. Two excitation wavelengths, 488 and 458 nm, and two emission bands, green and red, provided the three channels (cyan, green and red) required for ratio analyses (detailed in Methods). Global fitting (Methods, eq. 2) of R_{pH} values obtained from both cell lines provided a unique pH calibration curve (Figure 2a). Instead, Cl^- calibration could not be parametrized into a single reference curve, because chloride K_d of GFP-based biosensor is strongly pH-dependent[22]. Using the single 458-nm excitation, we acquired R_{Cl} values in HEK293 (Figure 2b) and in SK-N-SH (Supplementary Figure S11) cells at increasing amount of Cl^- concentration for various pH values. By fitting LSSmClopHensor Cl^- titration with eq. 3, we determined the dependence of chloride K_d on pH, which can be modeled according to the cooperative binding of H^+ and Cl^- to E^2GFP-based biosensors[30,37] as follows.

$$K_d(pH) = K_d^1 \frac{1 + 10^{pK_a - pH}}{10^{pK_a - pH}} \qquad (1)$$

where K_d^1 is the Cl^- dissociation constant of the fully protonated form of LSSmClopHensor; an intrinsic property of the sensor that together with the pK_a characterize the binding equilibria of LSSmClopHensor in solution. Using data from both cell lines for a global fit, we obtained a reference function for the dependence of the chloride K_d on pH (Figure 2c). Finally, the last parameter required by our calibration scheme was the setup dependent parameter R_{Cl}^0, estimated by clamping cells at $[Cl^-]$ = 0 mM. We recorded R_{Cl}^0 values in a wide pH range for both cell lines and obtained a weighed average value of 1.03 ± 0.19 (Figure 2d). Following the determination of three setup-dependent (R_{Cl}^0, R_A and R_B) and two LSSmClopHensor intrinsic (pK_a = 6.64 ± 0.12 and K_d^1 = 14 ± 3 mM) parameters, the following operational order settled

pH and Cl^- concentration maps: for each pixel of segmented cells (1) we assigned a pH value using the measured R_{pH} value and the pH calibration curve in Figure 2a; (2) then we calculated a chloride K_d value using eq. 1; and finally (3) we assigned a Cl^- concentration value using the measured R_{Cl} value and eq. 3 (Figure 2e and Figure 2f). The narrow pixel-by-pixel distribution reveals the precision of LSSmClopHensor for pH and Cl^- measurements (Figure 2g and Figure 2h).

We next investigated how the Cl^- is distributed both in cellular compartments and from cell to cell. We performed direct measurements of intracellular Cl^- concentration and pH in model neuronal SK-N-SH cells under physiological conditions (Figure 3). Distribution of Cl^- concentrations was narrow in SK-N-SH cells, peaking at 8.0 ± 4.1 mM (mean ± SD, N=37). On the contrary, we observed a broader distribution of intracellular Cl^- concentration in HEK293 cells (24 ± 12 mM, N=44). Intracellular pH values were 7.17 ± 0.13 (mean ± SD, N=37 cells) and 7.29 ± 0.18 (N=44 cells) for SK-N-SH and HEK293 cells, respectively. Our finding showing a lower Cl^- concentration in SK-N-SH than in HEK293 cells is in agreement with intracellular Cl^- values reported for neuronal cell lines[21,44,45] and other renal cell lines[21,46], and suggest the presence of mechanisms for a tight control of intracellular Cl^- in model neuronal cells.

Dynamic chloride imaging in neocortical brain slices. Lastly, we extended the use of LSSmClopHensor to monitor dynamic changes of Cl^- and H^+ concentration in neocortical neuron networks in ex vivo preparations. Electroporation *in utero* was performed in Sprague-Dawley rats at embryonic day 17 targeting progenitors of pyramidal neurons committed to layers II/III of the cortex. LSSmClopHensor showed a sustained and uniform expression - driven by the CMV early enhancer/chicken β actin (CAG) promoter - in the target neurons (Figure 4a; Supplementary Figures S12).

Neuronal somas and processes were imaged while performing synchronous electrophysiological recordings of local field potentials (LFP). We monitored pH and Cl^- concentration in real time during spontaneous and induced epileptic seizure like discharges (SLDs). Epileptiform activity was induced with 4-aminopyridine (4-AP; 50-100 µM), reduced Mg^{2+} (0.5 mM) and local NMDA brief applications as previously reported[47–49]. A total of 7 somas and 14 dendrites were imaged during successive SLDs from 9 slices. Figure 4 shows a typical experiment with the pH and Cl^- concentration calculated in a neuronal dendrite during 5 consecutive SLDs. Data showed an initial pH value close to 7.15 and a Cl^- concentration below 5 mM, in accordance with values from the SK-N-SH cells and from neurons[44]. SLDs produced an alteration in the fluxes of H^+ and Cl^- at the plasma membrane, causing an intracellular acidification and Cl^- accumulation in the imaged neurons. This observation, in line with previously reported data[29,44,50], pointed out the power of LSSmClopHensor for intracellular pH and Cl^- concentration measurements *in ex vivo* brain tissue. We measured changes of intracellular pH and Cl^- concentration during different SLDs. We calculated pH decreases of (mean ± SD, N=21 recordings from 9 biological replicates) 0.31 ± 0.06 and Cl^- concentration increases of 8.9 ± 3.8 mM (Figure 4).

Overall our data revealed that, compared to current methods to measure intracellular Cl^-, LSSmClopHensor represents a substantial advancement in several regards. Current electrophysiological methods provide only indirect estimates of Cl^- concentrations by measuring the reversal potential; they are invasive and difficult to use *in vivo*. Non-invasive chemical indicators have been widely used to measure Cl^- homeostasis, but their loading in living cells is difficult and are retained within the cells for only brief periods[51]. On the contrary, biosensors, which currently are all based on GFP variants with high affinity for Cl^-, can be targeted to specific sub cellular compartments and permanently retained within cells.

The broadly used Clomeleon[24] and improved variants are all based on the FRET occurring between a cyan donor and a chloride-sensitive acceptor YFP. Therefore, local pH changes impair their accuracy by altering the Cl^- affinity of the YFP moiety as well as the FRET efficiency. Changes in pH indeed affect the brightness of donor and acceptor, and thus make it difficult to predict the effect on the efficiency of the FRET process[52]. In neuronal cells, Cl^- fluxes are closely linked to the pH changes caused by the opening of GABA and glycine receptors generating activity-dependent fluxes of bicarbonate[50,53]. For this reason all Clomeleon derived biosensor need independent means to correct measured Cl^- concentration for concomitant pH variations. Unfortunately, this also applies to the recently developed SuperClomeleon, optimized for improved Cl^- affinity and signal-to-noise in cells[26]. On the contrary, LSSmClopHensor allows for precise quantification of intracellular Cl^- by measuring and removing pH bias on cell-by-cell basis alike the original ClopHensor. Furthermore, ClopHensor expression in neural cell can result in highly heterogeneous intracellular red aggregates, probably, as a consequence of DsRed aggregation in the cytosol and subsequent transport into lysosomes[54]. This problem has been recently circumvented by the substitution of DsRed with tandem dimer tomato (tdTomato), a bright dimer (66 kDa) red fluorescence protein, and the generation of ClopHensorN[44]. LSSmClopHensor maintain the same size of the original ClopHensor by using a monomeric red FP. Moreover, LSSmClopHensor allows for faster than ClopHensorN acquisition rates, thanks to the use of a single pH-independent excitation wavelength (458 nm) to measure Cl^- concentration. Thus, Cl^- ratio of LSSmClopHensor is also free from the biases resulting from intensity fluctuations in the excitation light source, an advantage that up to now was recognized only in sensors ratiometric in emission like Clomeleon.

Conclusions. Using a red long Stokes shift (LSS) FP and a chloride-sensitive green FP, we

have successfully developed a new genetically encodable chloride biosensor, LSSmClopHensor. We proved that a single excitation band is sufficient to optimally excite both green and red FP and exploit the ratio between their emissions for measuring intracellular Cl^-. The use of LSS FP in FRET-based biosensors will prove useful in the development of future biosensor, which will avoid biases in FRET efficiency calculations generated by changes in intracellular pH.

We have shown that LSSmClopHensor can be used to quantify simultaneously intracellular pH and Cl^- concentration in cell lines. Next we were able to monitor the dynamic changes of intracellular Cl^- (accumulation) and pH (acidification) during epileptiform activity in *ex vivo* cortical brain slices. Thus, we expect LSSmClopHensor to have wide use in imaging studies, in *ex vivo* and potentially also in *in vivo*, investigating the role of Cl^- and H^+ in the cellular physiology and physiopathology.

METHODS

DNA constructs and cloning. Nucleotide sequence for LSSmKate2, fused at the N-term to the polypeptide linker "ASGGGGGLVPRGSASGA", was codon-optimized for expression in mammalian cells using the OptimumGene algorithm (GenScript, Inc.), and cloned into pUC57 plasmid between BamHI and XbaI unique restriction sites (see Supplementary Information). The mammalian expression vector pcDNA3-LSSmClopHensor was obtained by subcloning the BamHI-XbaI fragment into pcDNA3-ClopHensor (Addgene #25938) to replace DsRed-monomer. The bacterial expression vector pET21-LSSmClopHensor was obtained by PCR amplification from pcDNA3-LSSmClopHensor using the primers NheI-E2-fw (5'-CTAGCTAGCGTGAGCAAGGGCGAGGA-3') and XhoI-LSS-rv (5'-CCGCTCGAGGCGATGGCCCAGCTT-3') for insertion into the multiple cloning site of pET21b vector (Novagen). Digestions with NheI and XhoI restriction enzymes were performed following the manufacturer's instructions (New England Biolabs). Bacterial expression vector for LSSmKate2 was prepared according the following procedure: sequence encoding LSSmKate2 was PCR-amplified from the pUC57-E2GFPLSSmKate2 plasmid using primers NheI-LSS-fw (5'-CTAGCTAGCGTGAGCGAACTGATTAAGGAG-3') and XhoI-LSS-rv (5'-CCGCTCGAGGCGATGGCCCAGCTT-3'). The insert was digested with NheI and XhoI restriction enzymes following the manufacturer's instructions (New England Biolabs).

Spectroscopy analysis of proteins *in vitro*. Recombinant LSSmClopHensor and LSSmKate2 were expressed in E. Coli BL21 (DE3) strain (Invitrogen) and purified by His-tagged affinity chromatography. Starter cultures were grown overnight in LB Broth (Sigma Aldrich) containing 100 mg/mL ampicillin (Sigma Aldrich) at 37°C. Bacterial cultures were pelleted

24 hours after induction with 1 mM isopropyl β-D-1-thiogalactopyranoside (IPTG) (Sigma Aldrich) at 30°C. Purification by affinity was carried out using HIS-Select™ Cartridges (Sigma Aldrich) following the manufacturer's instructions and collecting elution in 2-mL fractions. Chloride-free buffers were used in all the chromatography steps ensuring the absence of Cl^- from all preparations. If necessary, protein preparations were concentrated using centrifugal filter devices (Amicon Ultra-15, Millipore)

Absorption spectra were recorded using a steady-state spectrophotometer (model V-550 UV/VIS, Jasco, Inc.) equipped with a temperature-controlled cell holder. Fluorescence steady-state data were measured using an EnSpire spectral scanning multimode reader fluorometer (PerkinElmer) with 96-well black bottom plates (PerkinElmer, catalog # 6005279). Temperature was set at 20°C and 37°C and well volume was kept at 300 µL. Fluorescence intensities were collected with 100 numbers of flashes. Emission spectra were realized with excitation wavelength of 458 or 488 nm. Excitation spectra were recorded with an emission wavelength of 520 nm. Excitation and emission bandwidths were set both at 10 nm. Fluorescence spectra for pH titration were collected at 37°C using a Fluoromax-4 fluorescence spectrophotometer (Horiba) with excitation and emission bandwidths set at 5 nm.

pH and chloride imaging analysis. The combined pH and chloride ratio analysis was based on the acquisition of three fluorescence signals: cyan channel with excitation at 458 ± 10 nm and emission at 525 ± 25 nm; green channel with excitation at 482 ± 18 nm and emission at 525 ± 25 nm; and red channel with excitation at 458 ± 10 nm and emission at 610 ± 30 nm. For the calculation of Cl^- concentration and pH values two ratios were defined: R_{Cl} as red-over-cyan and R_{pH} as green-over-cyan. Ratio imaging analysis was performed as previously described[30] with the difference that no correction for fluctuation in the excitation intensity were required in this study, because a single light source (xenon lamp or argon laser) was used

with a 3-channel (cyan, green and red) image acquired within brief intervals (1-2 s). Briefly, to estimate the pK_a of LSSmClopHensor from pH titration data we used the following equation:

$$R_{pH} = \frac{R_B + R_A 10^{pK_a - pH}}{1 + 10^{pK_a - pH}} \qquad (2)$$

where R_A and R_B are the plateau values for R_{pH} at acidic and basic conditions, respectively. To estimate K_d from Cl^- titration data, we used equation (3)

$$R_{Cl} = \frac{R_{Cl}^0}{1 + \frac{[Cl]}{K_d}} \qquad (3)$$

where R_{Cl}^0 is the value of R_{Cl} at [Cl^-] = 0, a pH-independent and setup-dependent parameter. Accordingly, pH and Cl^- concentration maps were computed pixel-by-pixel using respectively the following equations 4 and 5.

$$pH = pK_a + \log\left(\frac{R_{pH} - R_A}{R_B - R_{pH}}\right) \qquad (4)$$

$$[Cl] = K_d(pH)\frac{R_{[Cl]}^0 - R_{Cl}}{R_{Cl}} \qquad (5)$$

To remove bleed-through in every channel, we calculated the intensity ratio of bleed-through in every emission channel using E^2GFP and LSSmKate2 proteins separately in independent experiments and varying intracellular pH in the range from 5.2 to 7.9 (Supplementary Figures S13, S14 and Table S1). The resulting images, corrected for bleed-through were then used to perform ratio analysis.

Fluorescence microscopy and image analysis. Images from cultured cells were recorded using a wide field microscope (iMIC, Till Photonics). Specimens were sequentially excited using a high stability 150 W xenon lamp (Oligochrome, Till Photonics) equipped with a fast filter switching device and the two required excitation filters: FF02-482/18-25 (Semrock), and

the laser clean-up filter z 458/10x (Chroma). A dual band dichroic mirror Di01-R488/561 (Semrock) was hosted in the filter cube. Emitted fluorescence was collected from 1.2 NA, 60X water immersion objective and split (at about 560 nm) into green and red channels using a single band dichroic mirror (FF560-Di01, Semrock) mounted into a dichrotome device (Till Photonics). The split channels were then simultaneously projected onto half of the electron multiplied charged-coupled device (Ixon Ultra 897; Andor Technologies). The three channels required by ratiometric analysis were thus recorded alternating between two excitation filters. Imaging of rat cortical brain slices was performed using a confocal laser scanning microscope (TCS SP5-RS, Leica) with a time frame acquisition of 0.995 s (seven line average). Excitation wavelengths were sequentially switching between 458 an 488 nm; emission bands were set from 498 to 560 nm and from 560 to 720 nm for the green and red channels, respectively. The setup was also equipped with a CCD camera for differential interference contrast images. All experiments were performed in layer II/III.

Image processing was performed using custom Fiji macros. Images were filtered with Gaussian filter (sigma=1.5). Mean background fluorescence was measured in empty regions and subtracted to all images. Images were semi-automatically segmented on the basis of pixel intensity using the isodata algorithm (*getAutoThreshold* method). Masked images were then used to discriminate regions of interest (cells) and prevent artifacts arising from dividing background by background values.

Cell culture and calibration. HEK 293 cells and SK-N-SH cells were cultured in Dulbecco's modified Eagle's medium (DMEM) (Sigma-Aldrich) supplemented with 10% Fetal Bovine Serum (FBS) (Sigma-Aldrich), 2 mM L-glutamine (Sigma-Aldrich), 100U/mL penicillin (Sigma-Aldrich) and 100mg /mL streptomycin (Sigma-Aldrich) in a humidified 5% CO_2 incubator at 37°C. All cells were transfected using Effectene reagent (Qiagen) following

manufacturer protocol. For differentiation, SK-N-SH cells were seeded to a confluence of approximately 30% in DMEM supplemented with 5% FBS, 2 mM L-glutamine, 100 U/mL penicillin, 100 mg/mL streptomycin and 10 μM retinoic acid (Sigma-Aldrich). The medium was changed every two days adding fresh retinoic acid. Differentiation was usually completed in 6 to 8 days when cell soma assumed a fusiform to triangular shape and elongation of slender neuritic processes was observed[55]. For SK-N-SH cell transfection the manufacturer protocol was adapted as follows: we doubled the amount of DNA and incubated transfection cocktail overnight in DMEM containing FBS (5%) and retinoic acid (10 μM).

Calibration in cells was realized as previously described[30]. The desired [Cl^-] and pH were controlled by equilibrating extra- and intracellular ion concentrations using the K^+/H^+ exchanger nigericin (5 μM), the protonophore carbonyl cyanide p-chlorophenylhydrazone (CCCP) (5 μM), the K^+ ionophore valinomycin (5 μM) and the Cl^-/OH^- exchanger tributyltin chloride (10 μM) in the presence of high-K^+ 20 mM HEPES buffer containing 0.6 mM $MgSO_4$, 38 mM sodium gluconate and 100 mM potassium gluconate. Specified amount of gluconate anion was replaced by Cl^-; pH was adjusted with aliquots of NaOH. To avoid CO_2 dependent pH shifts during calibrations, cells were maintained in CO_2 free atmosphere at 37°C. Medium was replaced with proper buffer and changed five times every two minutes to ensure stabilization of intracellular ionic concentrations.

Brain slice preparations and *in utero* electroporation. All experiments involving animals were carried out in strict accordance with the guidelines established by the European Communities Council Directive and approved by the National Council on Animal Care of the Italian Ministry of Health. The number of animals used was reduced to the minimum necessary for an adequate statistical analysis.

Coronal cortico-hippocampal slices were prepared from postnatal day 16–22 electroporated

Wistar rats. Briefly, rats were deeply anesthetized with intraperitoneal injected Zoletil (40 mg/kg; Virbac). After decapitation, the brain was removed and transferred to ice-cold cutting solution containing (in mM): NaCl, 120; KCl, 3.2; KH_2PO_4, 1; $NaHCO_3$, 26; $MgCl_2$, 2; $CaCl_2$, 1; glucose, 10; Na-pyruvate, 2; and ascorbic acid, 0.6; at pH 7.4 (with 5% CO_2/95% O_2). Coronal slices were obtained by using a Leica vibratome VT1000S in the presence of the ionotropic glutamate receptor inhibitor kynurenic acid (2 mM). Slices were recovered for 20 min at 32°C and then kept at room temperature.

Standard in utero electroporation of layer II/III of the somatosensory cortex was performed as previously described[56]. Briefly, E17 timed-pregnant Sprague-Dawley rats were anesthetized with isoflurane (induction, 3.5%; surgery, 2.5%), and the uterine horns were exposed by laparotomy. The day of confirmation of vaginal plug was defined as E0, and the day of birth was defined as P0. The DNA (0.15-1.5 µg/µl in water) together with the dye Fast Green (0.3 mg/ml; Sigma) was injected (5-6 µl) through the uterine wall into one of the lateral ventricles of each embryo using a 30G needle (Pic indolor). Embryo's head was carefully held between tweezer-type circular electrodes (10 mm diameter; Nepa Gene) that were wet with PBS while held across the uterine wall. For the electroporation protocol, 5 electrical pulses (amplitude, 50 V; duration, 50 ms; intervals, 150 ms) were delivered with a square-wave electroporation generator (CUY21EDIT; Nepa Gene). After electroporation, the uterine horns were returned into the abdominal cavity, and the embryos were allowed to continue their normal development.

Electrophysiology and induction of epileptic activity. Brain slices were continuously perfused in a submerged chamber (Warner Instruments) at a rate of 3-4 ml min-1 with (in mM): NaCl, 120; KCl, 3.2; KH_2PO_4, 1; $NaHCO_3$, 26; $MgCl_2$, 0.5; $CaCl_2$, 2; glucose, 10; pH 7.4 (with 5% CO_2/95% O_2). Seizure like events were evoked in the presence of 4-AP (50-100

μM). Bath temperature was maintained at 30-32°C by an in-line solution heater and temperature controller (TC-324B, Warner Instruments). A pressure ejection unit (PDES, NPI Electronics) was used to apply a single or double pulse to NMDA (1 mM, Sigma Aldrich)-containing pipettes with a 3 s interval, a pressure of 4–10 psi, and a duration of 200-600 ms. Typical pipette resistance was 2–3 MΩ. The NMDA glass pipette included an $AgCl_2$ electrode for extracellular local field potential recordings. Field potential signals were filtered at 1 kHz, amplified by an AM-1800 amplifier (AM-systems) and sampled at 10 KHz with a Digidata 1440s interface and pClamp software (version 10, Molecular Devices). Spectrograms of local field potential recording, were performed with an algorithm written in Matlab (version R2008b) using logarithmic wavelet windows.

Statistical methods. Calibration parameters were defined by global fitting to eq. 2 and eq. 3 using QtiPlot Software (http://www.qtiplot.com). Statistical tests were performed using Scipy (http://scipy.org). The reported P values were calculated using either the two-sample Kolmogorov-Smirnov test for statistical difference in distributions or the two-tailed Student's *t* test. Cumulative frequency distribution plots were prepared using Seaborn (http://stanford.edu/~mwaskom/software/seaborn).

ASSOCIATED CONTENT

Supporting Information

Optimized sequence of LSSmKate2, amino acid sequence of LSSmClopHensor in pcDNA3.1+ and pET21b vectors. Influence of the ionic strength over pK_a. Supplementary Figures S1-S14. Supplementary Table S1-S2. This material is available free of charge via the Internet at http://pubs.acs.org.

AUTHOR INFORMATION

Corresponding Authors

*JMP Email: jmparedes@ugr.es *DA Phone: +390461314607. Email: daniele.arosio@cnr.it

Notes

The authors declare no competing financial interests.

Author contributions

JMP, AII, LRA and DA designed the sensor and *in vitro* experiments. JMP, AII, LRA, SSS and PA prepared LSSmClopHensor constructs. AII performed calibrations. JS and LC performed the *in utero* electroporation. LM and GL performed electrophysiological recordings in brain slices and, with JMP and AII performed the imaging in neurons. GC and GMR designed the brain slice and imaging experiment. JMP and DA wrote the manuscript. JMP prepared supplementary information. All authors reviewed the manuscript and participated in the discussion of the data.

ACKNOWLEDGMENTS

We gratefully acknowledge the financial support of Telethon Italy (Grant GGP10138), RESTATE Programme co-funded by the European Union under the FP7 COFUND Marie Curie Action - Grant agreement no. 267224 to JMP, MIUR (PRIN 2009XPTWM2) and University of Trento (Progetti di Ricerca 2014).

FIGURE CAPTIONS

Figure 1. Spectroscopy characterization of purified LSSmClopHensor. (a) Schematic representation of LSSmClopHensor. Monomer LSSmKate2 dimensions are derived from structural data (PDB code: 3nt3). (b) Excitation spectra at pH values 5.59, 6.01, 6.40, 6.71, 7.12, 7.54, 7.98, 8.42 and 8.72 (color coded from red to blue in the direction indicated by the arrow). Emission wavelength set at 520 nm, [Cl^-] = 0 mM and temperature at 37°C. The presence of a single isosbestic point was unambiguously identified at 458 nm. (c, d) Emission spectra collected at the same pH values, from 5.59 to 8.72; excitation wavelength set at 488 (in c) and 458 (in d) nm, [Cl^-] = 0 mM and temperature at 37°C. Color shaded areas represent the spectral bands used in the analysis. (e) pH ratio values calculated after integration of emission spectra from 500 to 550 nm (shaded spectral range in c and d). Fitting curve was drawn using eq. 2 in Methods and the following best fit parameters: R_A = 0.41 ± 0.03, R_B = 2.66 ± 0.04 and pK_a = 6.86 ± 0.03. (f) Emission spectra at the [Cl^-] values of 0, 10, 25, 50, 75, 100, 250, 500 and 1000 mM; excitation wavelength set at 458 nm, the isosbestic point, pH = 6.5 and temperature at 37°C. The arrow indicates increases in the [Cl^-]. (g) Chloride ratio values corresponding to the data and spectral ranges reported in f. Fitting curve was drawn using eq. 3 in Methods and the following best fit ± SD (from fit) parameters: R_{Cl}^0 = 1.12 ± 0.06 and K_d = 33.6 ± 5.0 mM.

Figure 2. pH and chloride imaging calibration in cells. (a) Green-to-cyan R_{pH} ratio values vs. pH for LSSmClopHensor expressed in HEK293 (black circles) and SK-N-SH (red squares) cells. Global fitting curve was drawn for the two datasets using eq. 2 in Methods and the following best fit parameters: R_A = 2.75 ± 0.11, R_B = 10.2 ± 0.3 and pK_a = 6.89 ± 0.06. Error bars are cell-to-cell standard deviation (N = from 20 to 25 cells). (b) Cyan-to-red R_{Cl} ratio

values vs. Cl^- concentration for LSSmClopHensor expressed in HEK293 cells at the pH values of 5.54, 6.15, 6.62, 7.35, 7.56 and 7.90, in the direction indicated by the arrow. Fitting curves were drawn using eq. 3 in Methods. (c) Cl^- dissociation constant K_d, determined as exemplified in b, vs. pH for LSSmClopHensor expressed in HEK293 (black circles) and SK-N-SH (red squares) cells. Fitting curve was drawn using eq. 1 with the following best-fit parameters: pK_a = 6.64 ± 0.12 and chloride K_d = 14.27 ± 3.5 mM. Error bars represent the best fit uncertainties. (d) R_{Cl}^0 of HEK293 (black circles) and SK-N-SH (red squares) cell lines clamped at various pH values and $[Cl^-]$ = 0 mM. Error bars represent the best fit uncertainties. (e) Representative pH maps of HEK293 cells clamped at $[Cl^-]$ = 0 mM and various pH values. (f) Representative $[Cl^-]$ maps of HEK293 cells clamped at pH = 6.6 and various $[Cl^-]$ values. (g) Distributions of pH values corresponding to cells reported in e. (h) Distributions of $[Cl^-]$ values corresponding to cells reported in f.

Figure 3. LSSmClopHensor measures physiological changes in intracellular pH and Cl^- concentrations. (a) Representative pH map for SK-N-SH cells. The inserts show the distribution (pixel-by-pixel) of pH values for the highlighted cells. (b) Representative $[Cl^-]$ map for SK-N-SH cells. (c) Cell-by-cell distribution of pH w values for SK-N-SH cells (top) and HEK293 cells (middle) represented with histograms and kernel density estimate curves. Black (HEK293) and red (SK-N-SH) lines were drawn from the best fit to a Gaussian distribution. Comparison of the cumulative distribution functions for the examined cell populations (bottom) indicated that the average pH of SK-N-SH cells is distributed in a range of significantly (p = 0.005 in a Kolmogorov-Smirnov test for statistical difference in distributions) smaller pH values. Two-sided t-test indicated an average pH significantly different between the cell lines (p = 0.0009; and using Welch's t-test p = 0.0007 for different sample variances). (d) Cell-by-cell distribution of $[Cl^-]$ values for SK-N-SH cells (top) and

HEK293 cells (middle) represented with histograms and kernel density estimate curves. Black (HEK293) and red (SK-N-SH) lines were drawn from the best fit to a Gaussian distribution. Comparison of the cumulative distribution functions for the examined cell populations (bottom) indicated that the distribution of intracellular Cl^- concentration was significantly different between SK-N-SH and HEK293 cells ($p = 1.6\times10^{-10}$ in a Kolmogorov-Smirnov test between distributions).

Figure 4. pH and chloride imaging and simultaneous LFP recording during epileptiform activity. (a) Fluorescence images of pyramidal neurons in layer II/III of temporal cortex expressing LSSmClopHensor showing E^2GFP emission (green), E^2GFP emission with excitation at isosbestic point (cyan) and LSSmKate2 emission (red). Scale bar 10 μm. (b) Measurements of Cl^- concentration (blue trace) and pH (green trace) changes over time from a neuronal dendrite expressing LSSmClopHensor. The black trace displays the LFP of five consecutive SLDs recorded during the imaging session. Cl^- concentration and pH values were recorded with a time interval of 990 ms and calculated as reported in Methods. (c) Spectrogram of the recorded LFP representing the dominant frequency during epileptic activity. (d) Zoomed traces from the second SLD of panel b.

REFERENCES

(1) Faundez, V., and Hartzell, H. C. (2004) Intracellular Chloride Channels: Determinants of Function in the Endosomal Pathway. *Sci STKE 2004*, re8.

(2) Hartzell, H. C., and Ruppersburg, C. C. (2013) Functional reconstitution of a chloride channel bares its soul. *PNAS 110*, 19185–19186.

(3) Wolosker, H., de Souza, D. O., and de Meis, L. (1996) Regulation of glutamate transport into synaptic vesicles by chloride and proton gradient. *J. Biol. Chem. 271*, 11726–11731.

(4) Hodgkin, A. L., and Horowicz, P. (1959) The influence of potassium and chloride ions on the membrane potential of single muscle fibres. *J Physiol 148*, 127–160.

(5) Maeno, E., Ishizaki, Y., Kanaseki, T., Hazama, A., and Okada, Y. (2000) Normotonic cell shrinkage because of disordered volume regulation is an early prerequisite to apoptosis. *Proc. Natl. Acad. Sci. 97*, 9487–9492.

(6) Okada, Y., and Maeno, E. (2001) Apoptosis, cell volume regulation and volume-regulatory chloride channels. *Comparative Biochemistry and Physiology Part A: Molecular & Integrative Physiology 130*, 377–383.

(7) Ransom, C. B., O'Neal, J. T., and Sontheimer, H. (2001) Volume-Activated Chloride Currents Contribute to the Resting Conductance and Invasive Migration of Human Glioma Cells. *J. Neurosci. 21*, 7674–7683.

(8) Schwab, A., Fabian, A., Hanley, P. J., and Stock, C. (2012) Role of Ion Channels and Transporters in Cell Migration. *Physiol. Rev. 92*, 1865–1913.

(9) Payne, J. A., Rivera, C., Voipio, J., and Kaila, K. (2003) Cation–chloride co-transporters in neuronal communication, development and trauma. *Trends in Neurosciences 26*, 199–206.

(10) Owens, D. F., and Kriegstein, A. R. (2002) Is there more to gaba than synaptic inhibition?

Nat Rev Neurosci 3, 715–727.

(11) Rivera, C., Voipio, J., Payne, J. A., Ruusuvuori, E., Lahtinen, H., Lamsa, K., Pirvola, U., Saarma, M., and Kaila, K. (1999) The K+/Cl|[minus]| co-transporter KCC2 renders GABA hyperpolarizing during neuronal maturation. *Nature 397*, 251–255.

(12) Alvarez-Leefmans, F. J. (2011) Intracellular Chloride Regulation, in *Cell Physiology Source Book: Essentials of Membrane Biophysics*, pp 221–259.

(13) Planells-Cases, R., and Jentsch, T. J. (2009) Chloride channelopathies. *Biochim. Biophys. Acta BBA - Mol. Basis Dis. 1792*, 173–189.

(14) Deidda, G., Bozarth, I. F., and Cancedda, L. (2014) Modulation of GABAergic transmission in development and neurodevelopmental disorders: Investigating physiology and pathology to gain therapeutic perspectives. *Frontiers in Cellular Neuroscience 8*.

(15) Tyzio, R., Nardou, R., Ferrari, D. C., Tsintsadze, T., Shahrokhi, A., Eftekhari, S., Khalilov, I., Tsintsadze, V., Brouchoud, C., Chazal, G., Lemonnier, E., Lozovaya, N., Burnashev, N., and Ben-Ari, Y. (2014) Oxytocin-Mediated GABA Inhibition During Delivery Attenuates Autism Pathogenesis in Rodent Offspring. *Science 343*, 675–679.

(16) Lemonnier, E., Robin, G., Degrez, C., Tyzio, R., Grandgeorge, M., and Ben-Ari, Y. (2013) Treating fragile x syndrome with the diuretic bumetanide: A case report. *Acta Paediatr. 102*, e288–290.

(17) Deidda, G., Parrini, M., Naskar, S., Bozarth, I. F., Contestabile, A., and Cancedda, L. (2015) Excitatory GABAergic transmission impairs synaptic plasticity and memory in Down syndrome. *Int. J. Dev. Neurosci. 47*, 36.

(18) Glykys, J., Dzhala, V., Egawa, K., Balena, T., Saponjian, Y., Kuchibhotla, K. V., Bacskai, B. J., Kahle, K. T., Zeuthen, T., and Staley, K. J. (2014) Local Impermeant Anions Establish the Neuronal Chloride Concentration. *Science 343*, 670–675.

(19) Wietek, J., Wiegert, J. S., Adeishvili, N., Schneider, F., Watanabe, H., Tsunoda, S. P., Vogt, A., Elstner, M., Oertner, T. G., and Hegemann, P. (2014) Conversion of Channelrhodopsin into a Light-Gated Chloride Channel. *Science 344*, 409–412.

(20) Berndt, A., Lee, S. Y., Ramakrishnan, C., and Deisseroth, K. (2014) Structure-Guided Transformation of Channelrhodopsin into a Light-Activated Chloride Channel. *Science 344*, 420–424.

(21) Bregestovski, P., Waseem, T., and Mukhtarov, M. (2009) Genetically encoded optical sensors for monitoring of intracellular chloride and chloride-selective channel activity. *Front Mol Neurosci 2*, 15.

(22) Bregestovski, P., and Arosio, D. (2011) Green Fluorescent Protein-Based Chloride Ion Sensors for In Vivo Imaging, in *Fluorescent Proteins II* (Jung, G., Ed.), pp 99–124. Springer Berlin Heidelberg, Berlin, Heidelberg.

(23) Wachter, R. M., and Remington, S. J. (1999) Sensitivity of the yellow variant of green fluorescent protein to halides and nitrate. *Curr. Biol 9*, R628–629.

(24) Kuner, T., and G. J Augustine. (2000) A Genetically Encoded Ratiometric Indicator for Chloride: Capturing Chloride Transients in Cultured Hippocampal Neurons. *Neuron 27*, 447–459.

(25) Markova, O., Mukhtarov, M., Real, E., Jacob, Y., and Bregestovski, P. (2008) Genetically encoded chloride indicator with improved sensitivity. *J Neurosci Methods 170*, 67–76.

(26) Grimley, J. S., Li, L., Wang, W., Wen, L., Beese, L. S., Hellinga, H. W., and Augustine, G. J. (2013) Visualization of Synaptic Inhibition with an Optogenetic Sensor Developed by Cell-Free Protein Engineering Automation. *J. Neurosci. 33*, 16297–16309.

(27) Arosio, D., and Ratto, G. M. (2014) Twenty years of fluorescence imaging of

intracellular chloride. *Front. Cell. Neurosci. 8*, UNSP 258.

(28) Pond, B. B., Berglund, K., Kuner, T., Feng, G., Augustine, G. J., and Schwartz-Bloom, R. D. (2006) The chloride transporter Na(+)-K(+)-Cl- cotransporter isoform-1 contributes to intracellular chloride increases after in vitro ischemia. *J Neurosci 26*, 1396–406.

(29) Lillis, K. P., Kramer, M. A., Mertz, J., Staley, K. J., and White, J. A. (2012) Pyramidal cells accumulate chloride at seizure onset. *Neurobiol. Dis. 47*, 358–366.

(30) Arosio, D., Ricci, F., Marchetti, L., Gualdani, R., Albertazzi, L., and Beltram, F. (2010) Simultaneous intracellular chloride and pH measurements using a GFP-based sensor. *Nat. Methods 7*, 516–U44.

(31) Navarrete, M., Perea, G., de Sevilla, D. F., Gómez-Gonzalo, M., Núñez, A., Martín, E. D., and Araque, A. (2012) Astrocytes Mediate In Vivo Cholinergic-Induced Synaptic Plasticity. *PLoS Biol 10*, e1001259.

(32) Brondi, M., Sato, S. S., Rossi, L. F., Ferrara, S., and Ratto, G. M. (2012) Finding a Needle in a Haystack: Identification of EGFP Tagged Neurons during Calcium Imaging by Means of Two-Photon Spectral Separation. *Front. Mol. Neurosci. 5*.

(33) Dzhala, V., Valeeva, G., Glykys, J., Khazipov, R., and Staley, K. (2012) Traumatic alterations in GABA signaling disrupt hippocampal network activity in the developing brain. *J Neurosci 32*, 4017–4031.

(34) Glykys, J., Dzhala, V. I., Kuchibhotla, K. V., Feng, G., Kuner, T., Augustine, G., Bacskai, B. J., and Staley, K. J. (2009) Differences in Cortical versus Subcortical GABAergic Signaling: A Candidate Mechanism of Electroclinical Uncoupling of Neonatal Seizures. *Neuron 63*, 657–672.

(35) Piatkevich, K. D., Malashkevich, V. N., Almo, S. C., and Verkhusha, V. V. (2010) Engineering ESPT Pathways Based on Structural Analysis of LSSmKate Red Fluorescent

Proteins with Large Stokes Shift. *J. Am. Chem. Soc. 132*, 10762–10770.

(36) Piatkevich, K. D., Hulit, J., Subach, O. M., Wu, B., Abdulla, A., Segall, J. E., and Verkhusha, V. V. (2010) Monomeric red fluorescent proteins with a large Stokes shift. *Proc. Natl. Acad. Sci. 107*, 5369–5374.

(37) Arosio, D., Garau, G., Ricci, F., Marchetti, L., Bizzarri, R., Nifosi, R., and Beltram, F. (2007) Spectroscopic and structural study of proton and halide ion cooperative binding to GFP. *Biophys. J. 93*, 232–244.

(38) Bizzarri, R., Arcangeli, C., Arosio, D., Ricci, F., Faraci, P., Cardarelli, F., and Beltram, F. (2006) Development of a novel GFP-based ratiometric excitation and emission pH indicator for intracellular studies. *Biophys. J. 90*, 3300–3314.

(39) Shaner, N. C., Steinbach, P. A., and Tsien, R. Y. (2005) A guide to choosing fluorescent proteins. *Nat. Methods 2*, 905–909.

(40) Boens, N., Qin, W., Basarić, N., Orte, A., Talavera, E. M., and Alvarez-Pez, J. M. (2006) Photophysics of the fluorescent pH indicator bCECF. *J Phys Chem A 110*, 9334–9343.

(41) Paredes, J. M., Crovetto, L., Rios, R., Orte, A., Alvarez-Pez, J. M., and Talavera, E. M. (2009) Tuned lifetime, at the ensemble and single molecule level, of a xanthenic fluorescent dye by means of a buffer-mediated excited-state proton exchange reaction. *Phys. Chem. Chem. Phys. 11*, 5400–5407.

(42) Ross, R. A., Spengler, B. A., and Biedler, J. L. (1983) Coordinate Morphological and Biochemical Interconversion of Human Neuroblastoma Cells. *JNCI J Natl Cancer Inst 71*, 741–747.

(43) Acosta, S., Lavarino, C., Paris, R., Garcia, I., de Torres, C., Rodríguez, E., Beleta, H., and Mora, J. (2009) Comprehensive characterization of neuroblastoma cell line subtypes reveals bilineage potential similar to neural crest stem cells. *BMC Dev. Biol. 9*, 12.

(44) Raimondo, J. V., Joyce, B., Kay, L., Schlagheck, T., Newey, S. E., Srinivas, S., and Akerman, C. J. (2013) A genetically-encoded chloride and pH sensor for dissociating ion dynamics in the nervous system. *Front Cell Neurosci 7*.

(45) Dzhala, V. I., Kuchibhotla, K. V., Glykys, J. C., Kahle, K. T., Swiercz, W. B., Feng, G., Kuner, T., Augustine, G. J., Bacskai, B. J., and Staley, K. J. (2010) Progressive NKCC1-Dependent Neuronal Chloride Accumulation during Neonatal Seizures. *J. Neurosci. 30*, 11745.

(46) Miyazaki, H., Shiozaki, A., Niisato, N., and Marunaka, Y. (2007) Physiological significance of hypotonicity-induced regulatory volume decrease: Reduction in intracellular Cl- concentration acting as an intracellular signaling. *Am J Physiol Ren. Physiol 292*, F1411–F1417.

(47) Losi, G., Cammarota, M., Chiavegato, A., Gomez-Gonzalo, M., and Carmignoto, G. (2010) A new experimental model of focal seizures in the entorhinal cortex. *Epilepsia 51*, 1493–1502.

(48) Gómez-Gonzalo, M., Losi, G., Chiavegato, A., Zonta, M., Cammarota, M., Brondi, M., Vetri, F., Uva, L., Pozzan, T., de Curtis, M., and others. (2010) An excitatory loop with astrocytes contributes to drive neurons to seizure threshold. *PLoS Biol. 8*, 800.

(49) Cammarota, M., Losi, G., Chiavegato, A., Zonta, M., and Carmignoto, G. (2013) Fast spiking interneuron control of seizure propagation in a cortical slice model of focal epilepsy. *J. Physiol. 591*, 807–822.

(50) Kaila, K., Voipio, J., Paalasmaa, P., Pasternack, M., and Deisz, R. A. (1993) The role of bicarbonate in GABAA receptor-mediated IPSPs of rat neocortical neurones. *J Physiol 464*, 273–289.

(51) Fukuda, A., Tanaka, M., Yamada, Y., Muramatsu, K., Shimano, Y., and Nishino, H.

(1998) Simultaneous optical imaging of intracellular Cl− in neurons in different layers of rat neocortical slices: Advantages and limitations. *Neuroscience Research 32*, 363–371.

(52) Jose, M., Nair, D. K., Reissner, C., Hartig, R., and Zuschratter, W. (2007) Photophysics of Clomeleon by FLIM: Discriminating excited state reactions along neuronal development. *Biophys. J. 92*, 2237–2254.

(53) Bormann, J., Hamill, O. P., and Sakmann, B. (1987) Mechanism of anion permeation through channels gated by glycine and gamma-aminobutyric acid in mouse cultured spinal neurones. *J Physiol 385*, 243–286.

(54) Katayama, H., Yamamoto, A., Mizushima, N., Yoshimori, T., and Miyawaki, A. (2008) GFP-like proteins stably accumulate in lysosomes. *Cell Struct. Funct 33*, 1–12.

(55) Gaitonde, S. V., Qi, W., Falsey, R. R., Sidell, N., and Martinez, J. D. (2001) Morphologic Conversion of a Neuroblastoma-derived Cell Line by E6-mediated p53 Degradation. *Cell Growth Differ 12*, 19–27.

(56) dal Maschio, M., Ghezzi, D., Bony, G., Alabastri, A., Deidda, G., Brondi, M., Sato, S. S., Zaccaria, R. P., Di Fabrizio, E., Ratto, G. M., and Cancedda, L. (2012) High-performance and site-directed in utero electroporation by a triple-electrode probe. *Nat Commun 3*, 960.

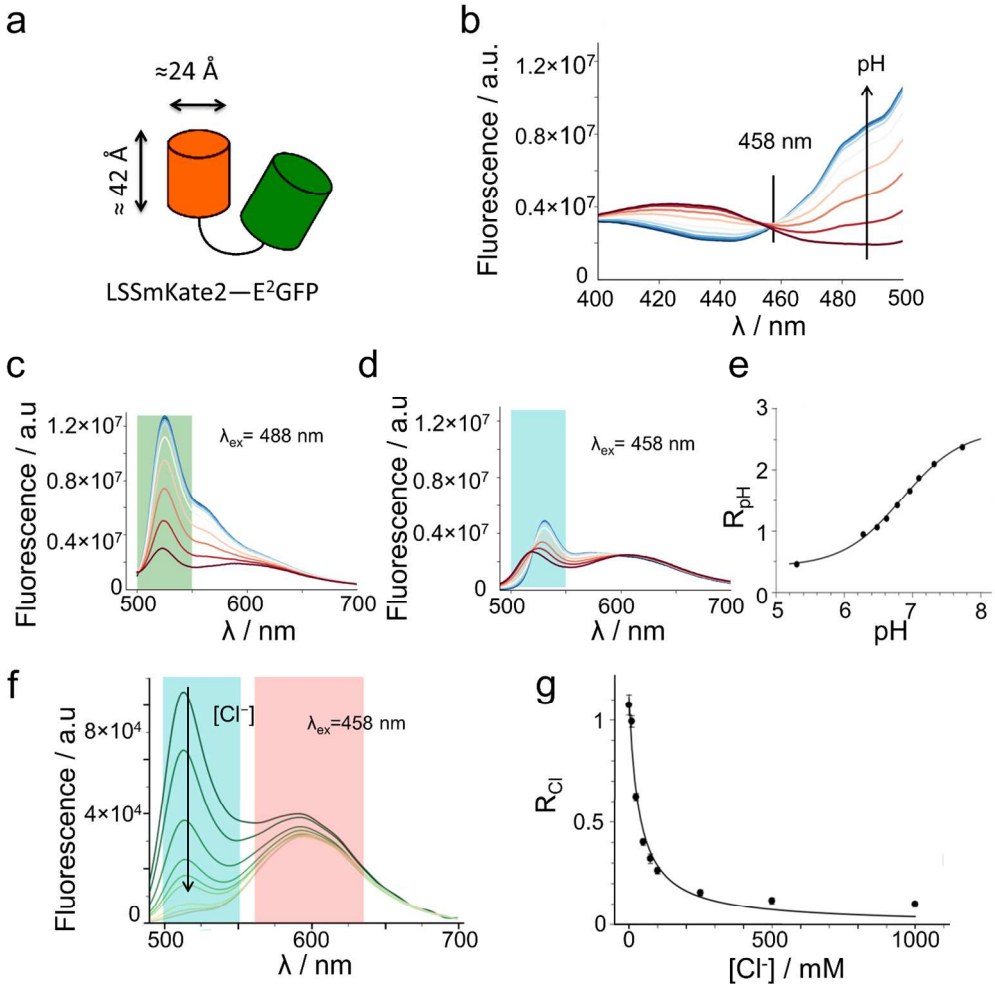

Figure 1. Spectroscopy characterization of purified LSSmClopHensor.
129x132mm (300 x 300 DPI)

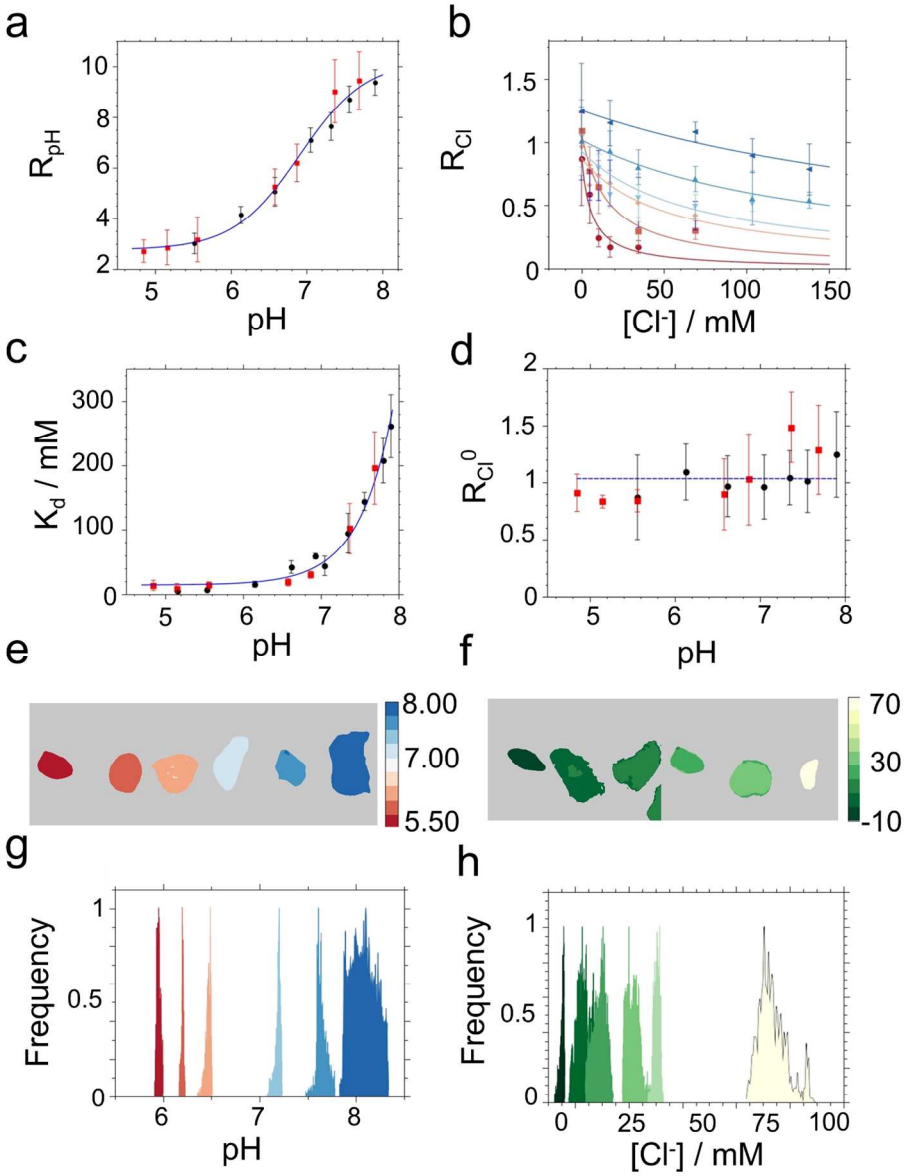

Figure 2. pH and chloride imaging calibration in cells.
130x168mm (293 x 293 DPI)

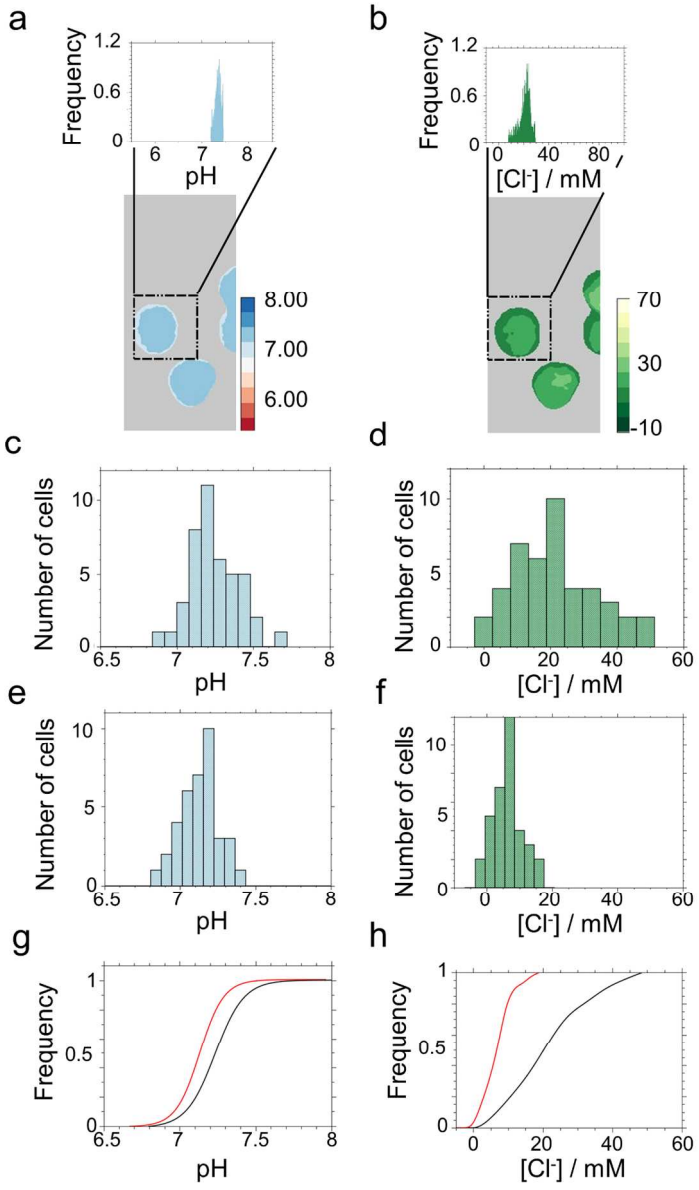

Figure 3. LSSmClopHensor measures physiological changes in intracellular pH and Cl- concentrations.
129x218mm (229 x 229 DPI)

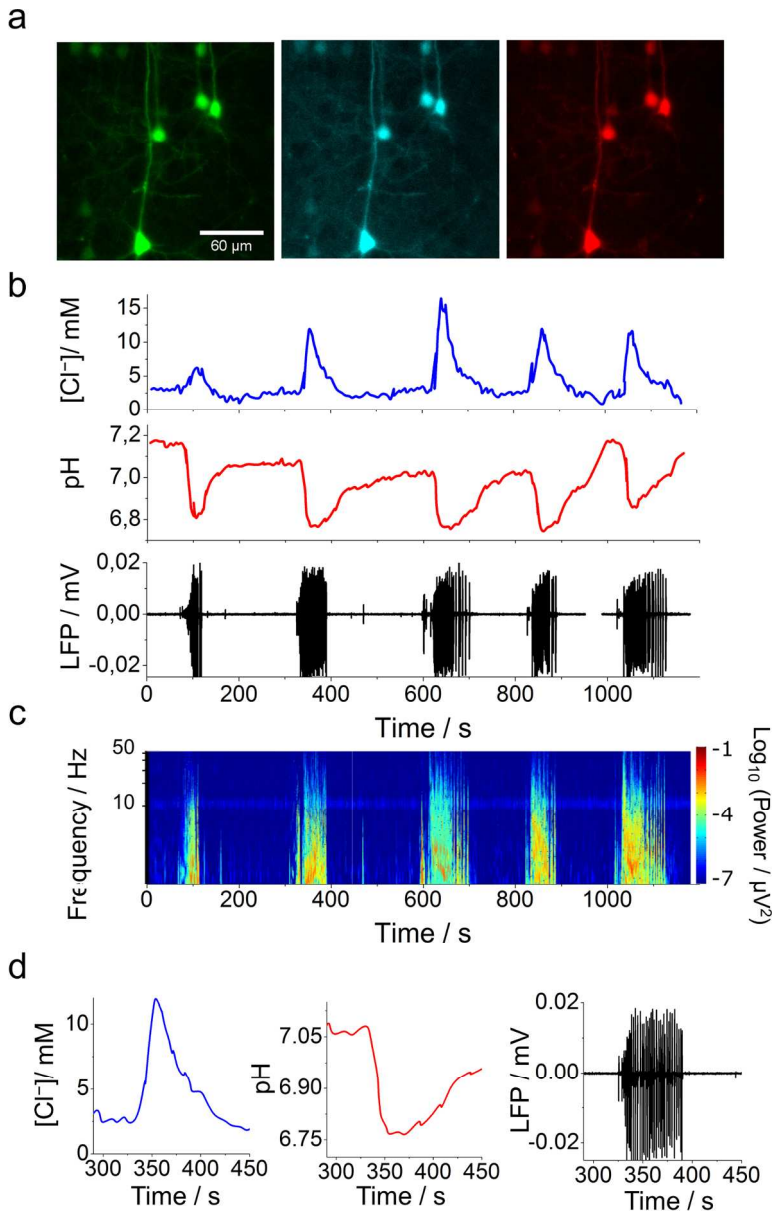

Figure 4. pH and chloride imaging and simultaneous LFP recording during epileptiform activity.
129x203mm (300 x 300 DPI)

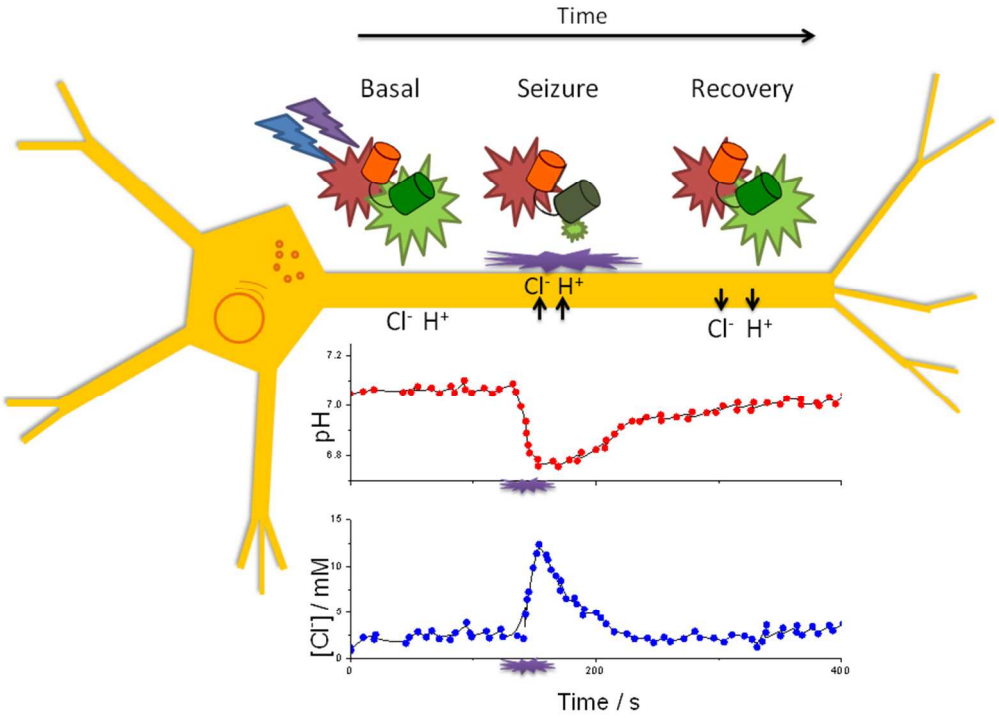
Time
Basal
Seizure
Recovery
Cl⁻ H⁺
Cl⁻ H⁺
Cl⁻ H⁺
pH
7.2
7.0
6.8
[Cl⁻] / mM
15
10
5
0
0
200
400
Time / s

ToC graphic